濟州大學校 尖端技術硏究所 論文集, 第12卷, 2號, pp.64-72, 2001. 12
Cheju Nat'l Univ. Res. Inst. Adv. Tech. Jour., Vol.12, No.2, pp.64-72, 2001. 12

Extended Kalman Filter Approach to Dynamic Electrical Impedance Tomography with Internal Electrodes

Suk-In Kang*, Kyung-Youn Kim*, Ho-Chan Kim*, Won-Churl Cho**,
Min-Chan Kim***, Sin Kim****, Heon-Ju Lee**** and Yoon-Joon Lee****

내부전극과 확장 Kalman Filter를 이용한 동적 전기임피던스 단층촬영 기법

강 숙 인* · 김 경 연* · 김 호 찬* · 조 원 철* · 김 민 찬***
· 김 신**** · 이 헌 주**** · 이 윤 준****

ABSTRACT

Electrical impedance tomography (EIT) is a relatively new imaging modality in which the internal impedivity distribution is reconstructed based on the known sets of injected currents through the electrodes and induced voltages on the surface of the object. We describe a dynamic EIT imaging technique for the case where the resistivity distribution inside the object changes rapidly within the time taken to acquire a full set of independent measurement data. In doing so, the inverse problem is treated as the nonlinear state estimation problem and the unknown state (resistivity) is estimated with the aid of extended Kalman filter in a minimum mean square error sense. In particular, additional electrodes are attached to the known internal structure of the object to enhance the reconstruction performance and generalized Tikhonov regularization technique is employed to mitigate the ill-posedness of the inverse problem. Computer simulations are provided to illustrate the reconstruction performance of the proposed algorithm.

Key Words : electric impedance tomography, Kalman filter, internal electrodes

* 제주대학교 전기전자공학과, 첨단기술연구소
Department of Electrical & Electronic Engineering, Research Institute of Advanced Technology, Cheju Nat'l Univ.
** 경도대학
Kyungdo Provincial College
*** 제주대학교 화학공학과, 첨단기술연구소
Department of Chemical Engineering, Research Institute of Advanced Technology, Cheju Nat'l Univ.
**** 제주대학교 에너지공학과, 첨단기술연구소
Department of Nuclear and Energy Engineering, Research Institute of Advanced Technology, Cheju Nat'l Univ.

I. INTRODUCTION

Over the past few decades, electrical tomography (ET) techniques have received much attention from both theoretical and experimental points of view since they can be used as an alternative imaging modality for monitoring tool in many fields of engineering. This is mainly due to the relatively

cheap electronic hardware requirements, noninvasive measurement sensing, and relatively good temporal resolution[1-3].

In electrical impedance tomography (EIT), the quantity to be imaged is actually the impedivity (inverse of admittivity) so that it includes both electrical capacitance tomography (ECT) and electrical resistance tomography (ERT). However, more frequently in EIT it assumed that the resistive part of the impedivity dominates and estimate only the resistivity (inverse of conductivity) distribution inside the object. The physical relationship between the internal resistivity and the surface voltages is governed by a partial differential equation (Laplace equation) with appropriate boundary conditions. Owing to the complexity of this relationship, it is in most cases impossible to obtain a closed-form solution for the resistivity distribution. Hence, various reconstruction algorithms have been developed in the literature to estimate the internal resistivity distribution of the object.

However, most of the reconstruction algorithms presented so far are mainly focused on the case where the internal resistivity of the object is time-invariant within the time taken to acquire a full set of independent measurement data. As is well known, the conventional EIT imaging techniques such as backprojection or modified Newton-Raphson (mNR) algorithm use a full set of voltage measurements for each image[4,5]. However, in some real applications such as biomedical and chemical processes, these static imaging techniques are often fail to obtain satisfactory temporal resolution for the reconstructed images due to the rapid changes in resistivity.

More recently, dynamic imaging techniques have been developed to enhance the temporal resolution of the reconstructed images in the situations where the resistivity distribution inside the object changes rapidly in time. In most of these techniques, the inverse reconstruction problem is treated as state estimation problem and the time-varying state is estimated with the aid of linearized Kalman filter (LKF)[6-10] or extended Kalman filter (EKF)[11,12].

Quite often in real situations, there are partially known fixed internal structures inside the object. These internal structures can be, for example, an impeller drive shaft or a mixing paddle in process vessels and an assembly of fuel rods in nuclear reactor. The internal structures inside the object may results in difficulties in the image reconstruction in EIT especially in the case where the high resistive region is near the conductive internal structure or vice versa[13,14]. The so-called masking effect in the reconstructed image may be significant for the high-contrast case. There are two ways to get around these difficulties: the one is to use the internal structure as additional electrodes[13,15,16] and the other is to take into account it as a priori information in the inverse procedure[14]. However, all of the above approaches are for the case where the resistivity distribution inside the object is time-invariant for one classical frame.

The purpose of the present work is to develop a dynamic EIT reconstruction algorithm for the case where the resistivity distribution inside the object changes rapidly within the time taken to acquire a full set of independent measurement data. To achieve the purpose, additional electrodes are attached to the known internal structure. The inverse problem is treated as the state estimation problem and the unknown state (resistivity) is estimated with the aid of the EKF in a minimum mean square error sense. In other to deal with the well-known ill-posedness of the EIT inverse problem, smoothness assumption is made and the generalized Tikhonov regularization technique is also introduced in the cost functional.

We carried out extensive computer simulations with synthetic data to illustrate the reconstruction

performance, and to investigate the effects of additional internal electrodes on the spatial and temporal resolution of the reconstructed images.

II. INVERSE SOLVER BASED ON THE EXTENDED KALMAN FILTER

In case where the resistivity distribution inside the object changes rapidly within the time taken to acquire a full set of independent measurement data, the conventional imaging techniques which need a full set of voltage measurements for each image often fail to obtain satisfactory temporal information on the resistivity distribution. We consider the underlying inverse problem as a state estimation problem to estimate rapidly time-varying distribution of the resistivity. In the state estimation problem, we need so-called the dynamic model which consists of the state equation, i.e., for the temporal evolution of the resistivity and the observation equation, i.e., for the relationship between the resistivity and boundary voltage.

In general, the temporal evolution of the resistivity distribution ρ_k in the object Ω is related by the nonlinear mapping. Here, the state equation is assumed to be of the linear form, of which the modeling uncertainty is compensated by the process noise

$$\rho_{k+1} = F_k \rho_k + w_k \tag{1}$$

where $F_k \in R^{N\times N}$ is the state transition matrix at time k and N is the number of finite elements in the FEM(finite element method). In particular, we take $F_k \equiv I_N$ where $I_N \in R^{N\times N}$ is an identity matrix, to obtain the so-called *random-walk* model. It is assumed that the process error, w_k is white Gaussian noise with the following covariance which determines the rate of changes in resistivity distribution

$$\Gamma_k^w = E[w_k \cdot w_k^T] \tag{2}$$

Let $U_k \in R^L$, defined as

$$U_k \equiv [U_k^1 U_k^2 \ldots U_k^L]^T \tag{3}$$

be the surface measurement voltages induced by the k^{th} current pattern and L is the number of electrodes attached on the surface of the object. Then the observation equation can be described as the following nonlinear mapping with measurement error

$$U_k = V_k(\rho_k) + v_k \tag{4}$$

where the measurement error v_k is also assumed to be white Gaussian noise with covariance

$$\Gamma_k^v = E[v_k \cdot v_k^T] \tag{5}$$

Linearizing (4) about the current predicted state $\rho_{k|k-1}$ we obtain

$$U_k = V_k(\rho_{k|k-1}) + J_k(\rho_{k|k-1}) \cdot (\rho_k - \rho_{k|k-1}) + H.O.T + v_k \tag{6}$$

where $H.O.T$ represents the higher-order terms which will be considered as additional noise, and $J_k(\rho_{k|k-1}) \in R^{L\times N}$ is the Jacobian matrix defined by

$$J_k(\rho_{k|k-1}) \equiv \left.\frac{\partial V_k}{\partial \rho}\right|_{\rho=\rho_{k|k-1}} \tag{7}$$

Let us define the pseudo-measurement as

$$y_k \equiv U_k - V_k(\rho_{k|k-1}) + J_k(\rho_{k|k-1}) \cdot \rho_{k|k-1} \tag{8}$$

Then we obtain the linearized observation equation by considering the $H.O.T$ in (6) as additional noise

$$y_k = J_k(\rho_{k|k-1}) \cdot \rho_k + \overline{v_k} \tag{9}$$

where $\bar{v}_k$ is composed of measurement error and linearization error and also assumed to be white Gaussian noise with covariance as

$$\bar{\Gamma}_k \equiv E[\bar{v}_k \bar{v}_k^T] \tag{10}$$

In Kalman filtering we estimate the state ρ_k based on all the measurements taken up to the time k. With the Gaussian assumptions the required estimate is obtained by minimizing the cost functional which is formulated based on the above state and observation equations (1) and (9), respectively. The cost functional for the conventional Kalman filter is of the form

$$G^a(\rho_k) = \frac{1}{2}\{\| \rho_k - \rho_{k|k-1} \|_{C_{k|k-1}^{-1}} + \| y_k - J_k(\rho_{k|k-1}) \cdot \rho_k \|_{(\bar{\Gamma}k)^{-1}}\} \tag{11}$$

where $C_{k|k-1} \in R^{N \times N}$ is the time-updated error covariance matrix, which is defined by

$$C_{k|k-1} \equiv E[(\rho_k - \rho_{k|k-1})(\rho_k - \rho_{k|k-1})^T] \tag{12}$$

In order to mitigate the inherent ill-conditioned nature of the EIT inverse problem, additional constraint is included in the cost functional

$$G^b(\rho_k) = \frac{1}{2}\{\| \rho_k - \rho_{k|k-1} \|_{C_{k|k-1}^{-1}} + \| y_k - J_k(\rho_{k|k-1}) \cdot \rho_k \|_{(\bar{\Gamma}_k)^{-1}} + \alpha \| R^* \rho_k \|\} \tag{13}$$

where α is regularization parameter which is chosen *a posteriori*, and R^* is modified regularization matrix. One popular conventional method for the choice for the regularization matrix R^* is a difference-type matrix on the basis of the generalized Tikhonov regularization technique[9] by the the smoothness assumptions in resistivity distributions. In this method, the resistivity distribution is parameterized such that

$$\rho = \sum_{n=1}^{N} \rho_n \chi_n \tag{14}$$

where χ_n is the characteristic function of the n^{th} finite element. The l^{th} row of R is

$$R_l^* = (0,0,\ldots,0,-1,0,\ldots,0,-1,0,\ldots,0,3,0,\ldots,0,-1,0,\ldots 0) \tag{15}$$

where 3 is located at the l^{th} column and -1 is placed in the columns corresponding to elements having common edge with the l^{th} element. Sometimes in real situations, there are partially known internal structures in which additional electrodes can be attached. In this case, the regularization matrix R^* is obtained from R by removing the -1 in Ref. 9 that corresponds to element having common edge with the known internal structure. In that case, the number 3 in (15) is also replaced by 2 since the smoothness assumption is violated between the known element and background.

Define the augmented pseudo-measurement $\bar{y}_k \in R^{(L+N)\times 1}$, and pseudo-measurement matrix, $H_k \in R^{(L+N)\times N}$ as

$$\bar{y}_k \equiv \begin{pmatrix} y_k \\ 0 \end{pmatrix} \tag{16}$$

$$H_k \equiv \begin{pmatrix} J_k \\ \sqrt{\alpha} R^* \end{pmatrix} \tag{17}$$

Then the cost functional, (13) can be rearranged as

$$G(\rho_k) = \frac{1}{2}\{\| \rho_k - \rho_{k|k-1} \|_{C_{k|k-1}^{-1}} + \| \bar{y}_k - H_k \rho_k \|_{(\Gamma_k)^{-1}}\} \tag{18}$$

where the augmented covariance matrix, $\Gamma_k \in R^{(L+N)\times(L+N)}$ is defined by

$$\Gamma_k \equiv \text{Blockdiag}[\bar{\Gamma}_k, I_N] \tag{19}$$

Minimizing the cost functional in (18) and solving for the updates of the associated covariance matrices

we obtain the recursive extended Kalman filter algorithm which consists of the following two steps[17]:

(i) *Measurement Updating Step (Filtering)*

$$G_k = C_{k|k-1}H_k^T[H_k C_{k|k-1}H_k^T + \Gamma_k]^{-1} \quad (20)$$

$$C_{k|k} = (I - G_k H_k)C_{k|k-1} \quad (21)$$

$$\rho_{k|k} = \rho_{k|k-1} + G_k[\bar{y}_k - H_k \cdot \rho_{k|k-1}] \quad (22)$$

(ii) *Time Updating Step (Prediction)*

$$C_{k+1|k} = F_k C_{k|k} F_k^T + \Gamma_k^w \quad (23)$$

$$\rho_{k+1|k} = F_k \rho_{k|k} \quad (24)$$

Hence, we can find the estimated state $\rho_{k|k}$ for the true state ρ_k in a recursive minimum mean square error sense for $k = 1.2.....rK$, where K is the number of the independent current patterns and r is the number of the classical frames. As a result, the only difference between the conventional EKF and the proposed EKF which includes *a priori* information for the partially known internal structure is that the dimension of the measurement updating procedure is increased.

III. COMPUTER SIMULATIONS

We carried out extensive computer simulations with synthetic data to evaluate the reconstruction performance of the proposed algorithm. In the simulations, the complete electrode model with the contact impedance of $0.005\Omega cm$ is employed.

The FEM meshes without internal electrodes used for the forward and inverse solvers are shown in Fig. 1 (a) and (b), respectively. In the forward computations we used the FEM with a mesh of 2400 elements and 1281 nodes. In the inverse computations, we used the FEM with a mesh of 600 elements and 341 nodes to reduce the computational burden. For the current injection and corresponding voltage measurement, traditional adjacent method[1] was employed through 16 boundary electrodes(L) so that the total measurement voltage data were $256(16\times16)$.

The FEM meshes with 4 internal electrodes used for the forward and inverse solvers are shown in Fig. 2 (a) and (b), respectively. In the forward computations we used the FEM with a mesh of 2544 elements and 1368 nodes. In the inverse computations, we used the FEM with a mesh of 636 elements and 366 nodes. We injected electrical current between 16 boundary electrodes and one of the internal electrodes and measured the corresponding voltage on the 20 electrodes(L) so that the total measurement voltage data were $320(20\times16)$.

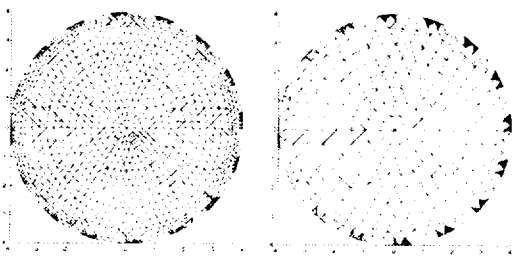

(a) (b)

Fig. 1. FEM meshes without internal electrodes used for (a) forward solver and (b) inverse solver.

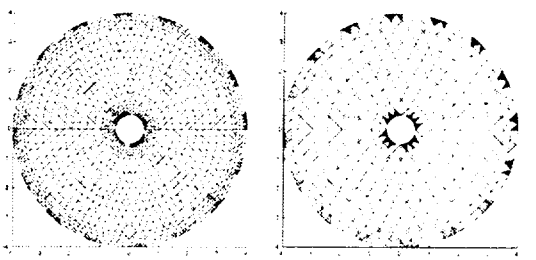

(a) (b)

Fig. 2. FEM meshes with 4 internal electrodes used for (a) forward solver and (b) inverse solver.

To compare the reconstruction performance. We used the static algorithm based on the modified Newton-Raphson algorithm with internal electrodes (mNR-IE)[16], dynamic algorithm based on the extended Kalman Filter (EKF)[12], and the Extended Kalman Filter with internal electrodes (EKF-IE) described in this paper. The parameters used for the three methods are as follows. The regularization parameter(α) is set to 0.5 in both simulations. The initial resistivity value is set to the same as the background value in all cases. For simplicity, it is assumed that the covariance matrices for all the EKFs are diagonal and time-invariant. The covariance matrix for process noise(Γ_k^w) is $10I_N$, the covariance matrix for measurement noise(Γ_k^v) is $0.0001I_L$ and the initial value for the state error covariance matrix ($C_{k|0}$) is I_N in both simulations.

3.1. The First Simulation

We generated the following sequence of resistivity distributions to simulate a dynamic situation. We assumed that there is known non-conductive circular structure (about 2 cm in diameter) located at the center of the domain, in which four electrodes are attached.

An almost circular-type target (resistivity of $600\Omega cm$) was moved abruptly to the opposite site through near the center after 4 current patterns in a circular domain(8cm in diameter, $300\Omega cm$ background resistivity) as depicted in the first column of Fig. 3.

Fig. 3 shows the reconstructed images for the three methods. The images in the second column are reconstructed by the EKF without internal electrodes. As can be seen clearly, the location (temporal resolution) of the moving target is rather misleading especially when the target is located near the non-conductive center of the domain(2nd and 3rd rows in the 2nd column). It seems that the error may be generated from the masking effect for the high-contrast. Also, the background was severely blurred by the non-conductive circular structure. The third column represents the reconstructed images from the EKF-IE. As can be expected, the reconstruction performance is improved qualitatively in terms of the temporal and spatial resolution. The reconstructed images obtained from the mNR-IE (fifth column) are also blurred and the information on the time-variability of the moving target is lost since it requires a full set of measurement data.

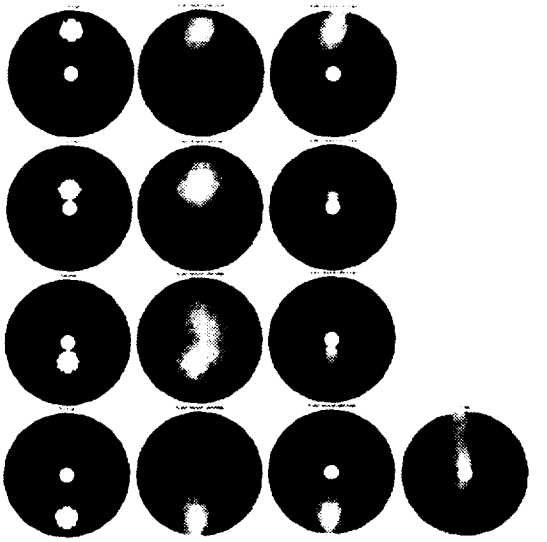

Fig. 3. Reconstructed images from the first simulation. (a) True target images. (b) reconstructed images by the EKF. (c) reconstructed images by the EKF-IE and (d) reconstructed images by the mNR-IE.

3.2. The second simulation

In the second simulation, we assumed the same scenario for the internal structure as in the first simulation. However, an almost circular-type target

(resistivity of 600Ωcm) was moved abruptly by 90° clockwise after every 4 current patterns in the same circular domain as in the first simulation (the first column of Fig. 4).

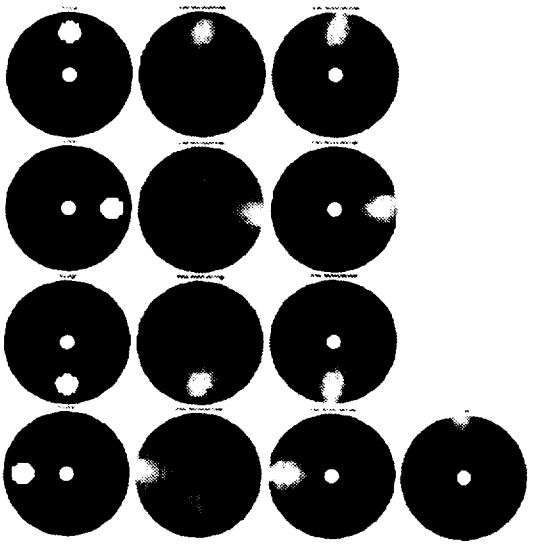

(a) (b) (c) (d)

Fig. 4. Reconstructed images from the second simulation.
(a) True target images. (b) reconstructed images by the EKF. (c) reconstructed images by the EKF-IE and (d) reconstructed images by the mNR-IE.

Figs. 4(b), (c) and (d) represent the reconstructed images obtained by the EKF, EKF-IE and mNR-IE, respectively. As can be seen, the images reconstructed by the EKF without internal electrodes are severely blurred in the homogeneous region (the second column). However, the reconstruction performance of the images obtained by the EKF-IE is enhanced qualitatively(the third column). Also, the temporal information for the abruptly changing targets is severely lost in the reconstructed images by the mNR-IE (the fourth column).

IV. CONCLUSION

Quite often in real situations, there are partially known fixed internal structures inside the object, in which additional internal electrodes could be attached. We have proposed a dynamic EIT reconstruction algorithm for the case where the fixed internal structure are known partially and the resistivity distribution of the other part inside the object changes rapidly within the time taken to acquire a full set of independent measurement data. In doing so, additional internal electrodes are attached to the known internal structures. EIT inverse problem is formulated as a state estimation problem and the state (resistivity distribution) is estimated with the aid of the EKF after the voltage measurements corresponding to each current pattern.

Computer simulation results showed that the proposed method produces qualitatively better reconstruction performance in the sense of the spatial and temporal resolution than do the other existing methods such as conventional EKF and mNR.

요 약

전기임피던스 단층촬영 기법은 상대적으로 최근에 개발된 영상화 기법으로, 대상물 표면으로 주입된 전류와 표면에서 측정된 전압으로 바탕으로 내부 임피던스 분포를 예측해내는 방법이다. 본 연구에서는 완전한 독립적인 측정 데이터를 얻기 전에 저항분포가 빠르게 천이하는 경우, 즉 동적 EIT 영상에 대한 기법을 소개하였다. 여기서, 역문제를 비선형 상태추정 문제로 취급하면서, 최소자승에 기초한 확장 Kalman filter 기법을 응용하였다. 특히, 기지의 내부 구조 정보를 이용하기 위하여 내부에 전극을 둠으로써 영상복원 능력을 향상시켰으며, Tikhonov regularization 기법을 도입하여 ill-posedness를 완화

하였다. 제안된 알고리즘의 성능을 평가하기 위하여 전산실험을 수행하였다.

ACKNOWLEDGEMENTS

This study was sponsored by Nuclear Academic Research Program by Ministry of Science & Technology (MOST).

REFERENCES

1) J. G. Webster. 1990. Electrical Impedance Tomography. Adam Hilger.

2) R. A. Williams and M. S. Beck. 1995. Process Tomography : Principles, Techniques and Applications. Butterworth-Heinemann. Oxford.

3) M. S. Beck and R. A. Williams. 1996. Process tomography : a European innovation and its applications. Meas. Sci. Tech., Vol.7. pp. 215-224.

4) D. C. Barber and B. H. Brown. 1984. Applied potential tomography. Journal of Physics E.. Vol. 17. pp.723-733.

5) T. J. Yorkey. J. G. Webster. and W. J. Tompkins. 1987. Comparing reconstruction algorithms for electrical impedance tomography. IEEE Trans. Biomed. Eng.. Vol.34. pp.843-852.

6) M. Vauhkonen. P. A. Karjalainen. and J. P. Kaipio. 1998. A Kalman filter approach to track fast impedance changes in electrical impedance tomography. IEEE Trans. Biomed. Eng.. Vol. 45. pp.486-493.

7) J. P. Kaipio. P. A. Karjalainen. E. Somersalo. and M.Vauhkonen. 1999. State estimation in time-varying electrical impedance tomography. Annals of New York Academy of Sciences. Vol. 873. pp.430-439.

8) P. J. Vauhkonen. M. Vauhkonen. T.Mäkinen. P. A. Karjalainen. and J. P. Kaipio. 2000. Dynamic electrical impedance tomography Phantom studies. Inverse Prob. Eng.. Vol.8. pp.495-510.

9) M. Vauhkonen. 1997. Electrical Impedance Tomography and Prior Information. Doctoral Dissertation. Dept. of Applied Physics. University Kuopio..

10) A. Seppanen. M. Vauhkonen. P. J. Vauhkonen. E.Somersalo. and J. P. Kaipio. 2001. State estimation with fluid dynamical evolution models in process tomography EIT applications. Inverse Prob.. Vol.17. pp.467-484.

11) K. Y. Kim. B. S. Kim. M. C. Kim and Y. J. Lee. 2001. On-line image reconstruction in dynamic electrical impedance tomography based on the extended Kalman filter. Proc. of Compumag-Evian (France). Vol.IV. pp.70-71.

12) K. Y. Kim. B. S. Kim. M. C. Kim. Y. J. Lee. and M.Vauhkonen. 2001. Image reconstruction in time-varying electrical impedance tomography based on the extended Kalman filter.. Meas. Sci. Tech.. Vol.12. No.8. pp.1032-1039.

13) R. A. Williams. X. Jia. and S. L. McKee. 1996. Development of slurry mixing models using resistance tomography. Powder Technology. Vol. 87. pp.21-27.

14) L. M. Heikkinen. M. Vauhkonen. T. Savolainen. K. Leinonen. and J. P. Kaipio. Electrical Process Tomography with known internal structures and resistivities. Inverse Prob. Eng. (in press).

15) G. M. Lyon and J. P. Oakley. 1993. A simulation study of sensitivity in stirred vessel electrical impedance tomography. In M. S. Beck. E. Campogrande. M. Morris. R. A. Williams. and R. C. Waterfall. editors. Tomography Techniques for Process Design and Operation. pp.137-146. Southampton UK. Computational Mechanics Publications.

16) L. M. Heikkinen. M. Vauhkonen. T. Savolainen. and J. P. Kaipio. 2001. Modeling of internal

structures and electrodes in electrical process tomography. Meas. Sci. Tech., Vol.12. pp. 1012-1019.

17) M. S. Grewal and A. P. Andrews. 1993. Kalman Filtering : Theory and Practice. Prentice Hall. Englewood Cliffs. New Jersey.